Article

Donor−Pyrene−Acceptor Distance-Dependent Intramolecular Charge-Transfer Process: A State-Specific Solvation Preferred to the Linear-Response Approach

Dipanwita Jana and Sankar Jana*

Cite This: ACS Omega 2020, 5, 9944−9956

Read Online

ACCESS | Metrics & More | Article Recommendations | SI Supporting Information

ABSTRACT: Photoinduced intramolecular charge-transfer (ICT) molecules are important in various applications such as a probe for single-molecule spectroscopy, cell imaging, laser dyes, biomarkers, solar cells, in photosynthesis, etc. Here, we report a new set of substituted pyrene dye molecules, *N,N*-dimethylamino nitrilo pyrene and its higher analogues, containing pull−push donor (D)−chromophore (π)−acceptor (A) functional groups with enhanced photophysical characteristics like oscillator strength, light-harvesting, and ICT properties. The excited-state ICT process has been established by quantum chemical calculations using the density functional theory method in vacuo and in solvents of different polarity and hydrogen-bonding ability using linear-response (LR) and state-specific (SS) solvation approaches with gradually increasing the D−A distance. The studied molecules show solvent polarity-dependent larger Stokes' shifts (3609−9016 cm^{-1}, in acetonitrile), higher excited-state dipole moments (11.7−16.8 Debye, in acetonitrile), higher possibilities of highest occupied molecular orbital (HOMO)−lowest unoccupied molecular orbital (LUMO) electronic transitions, etc., which support the occurrence of the excited-state ICT process. Here, we demonstrate how to increase the efficiency of the ICT process and also tune the ICT fluorescence maximum. We find that with a variation of the D−A distance, studied molecules show a noticeable effect on the spectroscopic and molecular properties such as the position of absorption and fluorescence band maxima, Stokes' shift, dipole moment, light-harvesting, and ICT properties. We also show that the SS solvation approach is more supportive than the LR method to the ICT process.

n= 0→DANP$_0$, 1→DANP$_1$, 2→DANP$_2$, 3→DANP$_3$

LUMO+1 · LUMO · HOMO · HOMO · DANP$_0$ · DANP$_3$
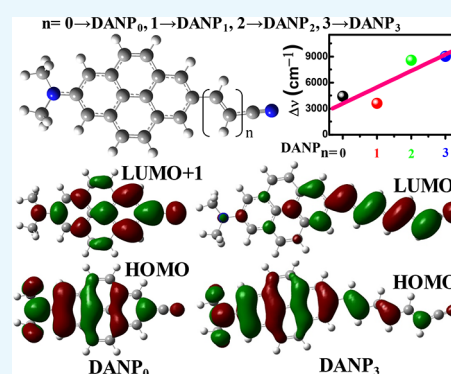
1. INTRODUCTION

The photoinduced intramolecular charge-transfer (ICT) process has been found to produce polarity sensitive emission in a number of push−pull systems where donor and acceptor groups are connected to a central aromatic chromophore (Scheme 1a).[1] A huge surge in the design and synthesis of such ICT compounds has been noted ever since the first observation of this behavior in the iconic molecule 4-(*N,N*-dimethylamino)benzonitrile (DMABN).[2] Lippert et al. first observed a dual anomalous fluorescence in polar solvents for the DMABN molecule, where the higher-energy emission originates from the locally excited (LE) state and the lower-energy emission from the polar solvent-stabilized charge-transfer (CT) state (Scheme 1b,c).[1,2] To date, varieties of ICT molecules have been studied due to their importance in various applications such as a probe for single-molecule spectroscopy, cell imaging, laser dyes, biomarkers, solar cells, etc.[3−8] ICT molecules also have a crucial role in biological light-harvesting processes, e.g., photosynthesis.[9,10] The ICT molecules containing a central benzene chromophore are mostly reported.[1,11,12] In addition to that, ICT molecules having naphthalene[13] and anthracene[14] rings with extra flexibility between the donor and acceptor are also found.[15−18] Recently,

few reports containing a pyrene chromophore with more complicated molecular structures are also observed.[19−21]

Generally, the ICT molecules show low quantum yield and low-intensity fluorescence spectral properties due to n → π* type of forbidden electronic transition.[22,23] For efficient applications of ICT molecules, it is recommended to have high quantum yield. At present, there are few commercial suppliers to provide the fluorescent ICT molecular probes with >60% quantum yield, which are also very expensive, thereby reducing their commercial viability.[24,25] On the other hand, most of the fluorophore probe molecules are excited within the ultraviolet region.[16,22,26] This is a limitation for the use of pyrene-based probe molecules in light microscopy and single-molecule spectroscopy for studying live cells and biomolecules like proteins, DNA, RNA, etc. For single-molecule spectroscopy, the photostable fluorescence molecular probe with very
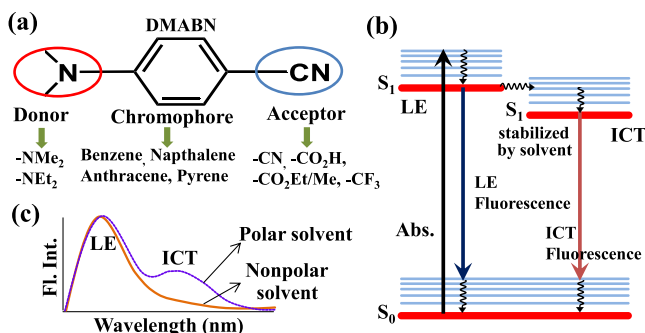
Scheme 1. General Chemical Structure of ICT Molecules, Schematic of Electronic Transitions and Fluorescence Spectra[a]


[a](a) Chemical structure of ICT molecules, the DMABN, and others by mentioning the donor, chromophore, and acceptor groups. (b) The electronic energy-level diagram for the dual emission LE and ICT in a polar solvent. (c) Sketch of fluorescence spectra of an ICT molecule in polar and nonpolar solvents to show the dual emission.

high quantum efficiency is recommended so that the photobleaching will be less by using very low energy excitation light.

To resolve the above issues, we computationally designed a new class of ICT molecules containing donor (NMe₂)−chromophore (pyrene)−acceptor (CN) groups with the variation of the D−A distance (Scheme 2). The pyrene

Scheme 2. Schematic Diagram of the Studied Donor−Acceptor-Substituted Pyrene ICT Molecules

n=0→DANP₀, n=1→DANP₁, n=2→DANP₂, n=3→DANP₃
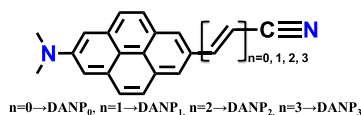
chromophore will help to increase the quantum yield by $\pi \rightarrow \pi^*$ type of allowed charge-transfer transition in addition to the weaker $n \rightarrow \pi^*$ type.[26−28] The gradual addition of π-conjugated alternate double and single bonds between the pyrene and nitrile groups will help to tune the absorption and fluorescence band maxima to the visible spectral range.[22,29] Experimental data for analogous pyrene molecules also support our computational findings.[21,26] The specific features of the pyrene charge-transfer molecules will attract attention due to a slower lifetime for real-time probe monitoring; the high quantum yield will help to use the probe even in a nanomolar concentration range to avoid excimer emission when measuring in a conventional fluorescence spectrometer.[30] Pyrene is already used as a biomarker for labeling biomolecules due to its good fluorescence character.[30−32] This probe also used in single-molecule spectroscopy and FRET study.[33,34] On the other hand, the pyrene-containing donor (D)−chromophore (π)−acceptor (A) organic dye has shown much improved photovoltaic performance than others.[28] As pyrene-chromophore-containing D−π−A groups can fulfill above criteria, therefore, development of a new class of pyrene ICT molecules and investigation of the D−A distance-dependent ICT phenomena are important and demanding.

The synthesis of 2,7-disubstituted D−π−A pyrene molecules is more expensive and complicated due to the availability of appropriate starting materials, catalysts and the presence of a

multistep synthetic process, which results in a low yield.[21,35] On the other hand, after the synthesis of the desired molecules, there remain some uncertainties as to whether these molecules will show the expected spectral properties. To avoid those uncertainties, we designed a series of donor−acceptor 2,7-disubstituted pyrene molecules and established the expected spectral properties using the computational methods and solvation techniques, which are more reliable to provide the results close to the experimental one.[21,27] In recent times, the state-specific (SS) calculation using a solvation model is more powerful to provide the ICT results than the linear-response (LR) calculation[27,36,37] using the Coulomb-attenuated B3LYP functional (CAM-B3LYP)[21,30,38] and conductor-like polarizable continuum model (CPCM).[21,30,39]

Here, we quantum chemically examined the photophysical properties and established the ICT phenomenon of the designed D−π−A molecules (Scheme 2) by calculating the spectroscopic parameters in different solvents using quantum chemical methods. We investigated the nature of the charge-transfer character and how it depends on the D−A distance and also the effect of the π electron-rich bulky pyrene chromophore on the ICT phenomenon. We further optimized the molecules in the gas phase and within different solvents with increasing polarity as well as the hydrogen-bonding character by the SS and the LR approaches through nonequilibrium and equilibrium solvation processes. Calculated ground- and excited-state geometries, dipole moments, Stokes' shifts, highest occupied molecular orbital (HOMO)−lowest unoccupied molecular orbital (LUMO) diagrams, etc. adequately support the charge-transfer nature and D−A distance-dependent charge-transfer property of the designed pyrene ICT molecules.

2. COMPUTATIONAL METHODS

2.1. Theoretical Background. The solute electron density of the ICT state differs significantly from that of the reference ground state and this electron density depends on the change of the dipole moment and stabilization of the state by surrounding solvent molecules. Therefore, the excited-state free energy critically depends on the solvent reorganization. During studying electronic processes like the formation and relaxation of excited states in solution, the solvent delay response has to be considered properly with respect to the ultrafast time scale of the excitation or emission processes. Therefore, consideration of the proper solvation model is important to get the accurate free energy of solvation. The approximated polarizable continuum model (CPCM)[40] and the polarizable continuum model (PCM)[41,42] are successful solvation methods among the others and their description are provided in the literature elaborately. Recently, the CPCM model has been widely used to get good results for long-range charge-transfer molecules.[21,30,38] In the CPCM model, the solvation free energy (ΔG_{sol}) expressed as follows by neglecting the other small-quantity terms.[39]

$$\Delta G_{sol} = \Delta G_{el} + \Delta G_{cav} + \Delta G_{dis} + \Delta G_{rep} \qquad (1)$$

where ΔG_{el}, ΔG_{cav}, ΔG_{dis}, and ΔG_{rep} are the electrostatic component, cavitation, dispersion, and repulsion terms of ΔG_{sol}. The electrostatic component can be calculated using the CPCM self-consistent reaction field (SCRF) method.[39] The cavitation term is calculated by using Pierotti's expression of the hard-sphere theory and applied for nonspherical cavities.[39]

Dispersion and repulsion terms are computed following Floris and Tomasi's procedure, with the parameters proposed by Callet and Claverie.[39]

Depending upon the reorientation of the solvent dipoles around the solute molecule, the CPCM approach involves two solvation cases, i.e., the equilibrium and the nonequilibrium. In the equilibrium condition, all of the electronic and the nuclear solvent degrees of freedom are in equilibrium with the electron density of the solute. Therefore, the apparent surface charges are computed by employing the static dielectric constant. Whereas for the nonequilibrium condition, only the electronic polarization of the solvent molecule is in equilibrium with the excited-state electron density of the solute and the apparent surface charges are separated into two sets of charges, representing the electronic polarization (fast) and nuclear components (slow) whose values are computed by using the optical and static dielectric constants, respectively. In the case of the absorption process, the solvent molecules are in nonequilibrium with the excited-state electron density; therefore, the vertical excitation energy is computed in terms of free energy by the following equation[27]

$$\Delta G_{abs} = G_{neq}^1 - G_{eq}^0 \tag{2}$$

where G represents the free energy. The superscript (1), (0) and subscript neq, eq denote the excited, ground states and nonequilibrium, equilibrium conditions, respectively.

As soon as the electronic excitation occurs, the solute molecule starts to relax toward the minimum of the excited-state potential energy surface. Simultaneously, the solvent molecules around the solute start to reorganize to reach the equilibrium with the excited-state electron density of the solute. As these two processes cannot be strictly decoupled, particularly when they exhibit similar time scales there is not a suitable single strategy to investigate all of the possible emission processes. To simplify this complex strategy, two limiting cases can be considered. Case 1: for the ultrafast excited-state decay, the equilibration of intramolecular degrees of freedom is faster than solvent equilibration and as a result, the emission occurs from the excited-state minimum. In that case, only the fast solvent degrees of freedom are in equilibrium with the excited-state density. Therefore, the ΔG_{em} can be computed in the same way as ΔG_{abs} in eq 2. Case 2: for molecules with very long excited-state lifetimes or strongly fluorescent compound, as in the case of donor–acceptor-substituted pyrene, it is possible to assume that all of the solvent degrees of freedom are in equilibrium with the excited-state density and the fluorescence can be computed by the following relation[41]

$$\Delta G_{em} = G_{eq}^1 - G_{neq}^0 \tag{3}$$

where the terms have usual significance as defined before. The expression for G_{eq} and G_{neq} reported elsewhere in the literature.[27,36,40,41]

2.2. Geometry Optimization. The ground- and excited-state energy optimization of all of the molecules (Scheme 2) was carried out by density functional theory (DFT) and time-dependent density functional theory (TD-DFT) methods, respectively, using Coulomb-attenuated functional, CAM-B3LYP and 6-311++G(d,p) basis set. The CAM-B3LYP functional provides better Hartree–Fock (HF) exchange correlation, starting from 0.19 Hartree–Fock (HF) and 0.81 Becke exchange interaction at the short range to 0.65 HF and 0.35 Becke exchange interaction at the long range.[43] Therefore, it is effective for both the pyrene and long-range charge-transfer systems, like our systems.[21,30] We selected the above-mentioned calculation method, functional, and basis set to obtain reliable results in comparison to the experimental data of similar types of molecules and also to balance the effective computational cost.[21,30,38] Even nowadays, quantum mechanical calculations of such types of molecules containing 47 atoms by using a 6-311++G(d,p) split valence basis set, which is equivalent to the triple-ζ basis set, containing diffusion function with polarization on hydrogen and heavy atoms are expensive mainly when the excited-state frequency calculations were performed using the solvent model. On the other hand, recent studies show that the CAM-B3LYP functional with the CPCM model provides better computational results when comparing with the experimental results for such types of D−π−A push−pull π-conjugated systems.[21] Also, the additional functional B3LYP was used for comparison, considering the SS and LR solvation approaches, as we applied for the CAM-B3LYP functional. The computational calculations were performed in vacuo and in different solvents with the variation of polarity and hydrogen-bonding abilities. We used a wide range of solvents: n-hexane (n-hex), dioxan (DOX), chloroform (CHCl$_3$), tetrahydrofuran (THF), acetonitrile (ACN), butanol (BuOH), ethanol (EtOH), methanol (MeOH), and water (H$_2$O) with their specified dielectric constants, as mentioned in the Gaussian 09 package.[44] All of the structures were optimized without freezing any parameters. To evaluate the solvent effect, the calculations were performed using the CPCM model without any constraints. The energy-optimized geometries were confirmed by frequency calculations without any imaginary frequencies. All of the computational works were carried out using Gaussian 09 suit program.[44] To visualize the results, the Gauss view 5 software was used.

2.3. Absorption and Fluorescence Band Positions, Light-Harvesting Property, and Solvatochromism. The absorption and fluorescence band positions were calculated in different solvents by seven consecutive stages, Scheme 3, and the data are presented considering state-specific and linear-response solvations. In the first stage, the ground-state geometry optimization was performed followed by frequency calculation. The second stage is the vertical excitation by a single-point TD-DFT calculation with linear-response solvation to know the excited state with a specific interest. The third is the state-specific solvation of the vertical excitation using TD-DFT calculation for the first excited state (S$_1$) by reading previously calculated ground-state (S$_0$) nonequilibrium solvation information. In the fourth stage, the excited-state geometry optimization was performed with the equilibrium condition and linear-response solvation. For this step, the parameters obtained from the checkpoint file of the second stage were used. The fifth stage is the most challenging and expensive step of excited-state frequency (S$_1$) calculation to confirm the excited-state geometry optimization. Sixth and seventh stages are the emission state-specific solvation and emission to the final ground state, respectively. To get the absorption band position with state-specific solvation, the obtained energy in the third stage after PCM correction was subtracted from the transition energy obtained in the first stage. Similarly, the fluorescence band position considering state-specific solvation was extracted from the energy difference between the sixth and the seventh stages (Scheme 3).

Scheme 3. Schematic Diagram of Equilibrium, Nonequilibrium, State-Specific, Linear-Response Solvation, Excitation, and Fluorescence Processes[a]
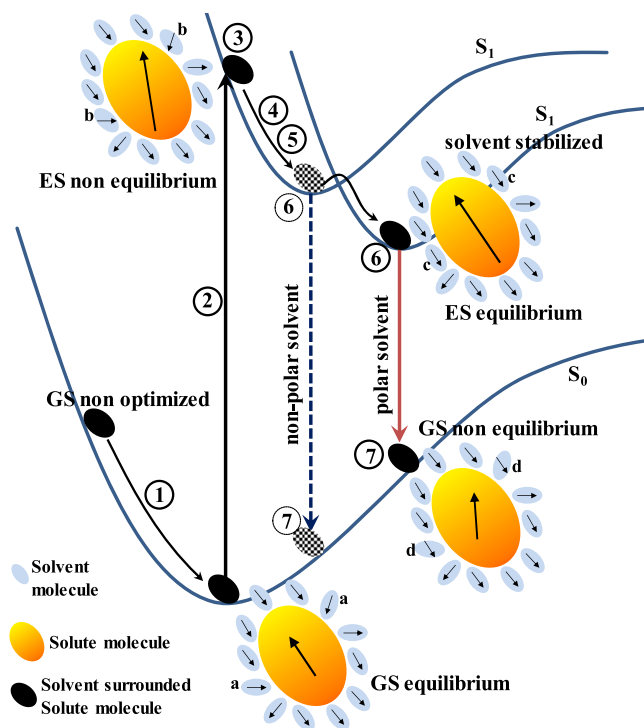
[a]The numbers within the circle represent different stages of the calculations. The dashed arrow, dotted circles, and dotted molecules indicate in nonpolar or less polar solvents. The arrow within the solute and the solvent molecules indicates the dipole moment. Solvent molecules, a, b, c, and d represent different equilibrium and nonequilibrium situations with respect to its previous state before the transition and the solute dipole after the transition.

The light-harvesting property of the investigated $DANP_n$ dye molecules has been studied by the calculation of the light-harvesting efficiency (LHE) using the following eq 4.[28]

$$\text{LHE} = 1 - 10^{-f} \tag{4}$$

where f is the calculated oscillator strength of $DANP_n$ molecules for the $S_0 \rightarrow S_1$ electronic transition by the absorption of light.

For the solvatochromic study, the Lippert–Mataga relation has been used, as shown in eq 5.[45] Stokes' shift ($\Delta\nu = \nu_a - \nu_f$) was plotted against the solvent parameter $\Delta f(\varepsilon_r, n)$ considering nonpolar n-hex to polar aprotic solvents with gradually increasing polarity. The nonpolar solvent n-hex was taken into account to show the inherent Stokes' shift of the studied molecules.

$$\nu_a - \nu_f = \frac{(\mu_e - \mu_g)^2}{2\pi\varepsilon_0 hc\rho^3} f(\varepsilon_r, n) \tag{5}$$

Where

$$f(\varepsilon_r, n) = \left[\frac{\varepsilon_r - 1}{2\varepsilon_r + 1}\right] - \left[\frac{n^2 - 1}{2n^2 + 1}\right]$$

ν_a, ν_f ε_r, and n are the absorption and the fluorescence band positions in cm^{-1}, the dielectric constant, and the refractive index of the medium, respectively. The terms h, ε_0, c, ρ, μ_g, and
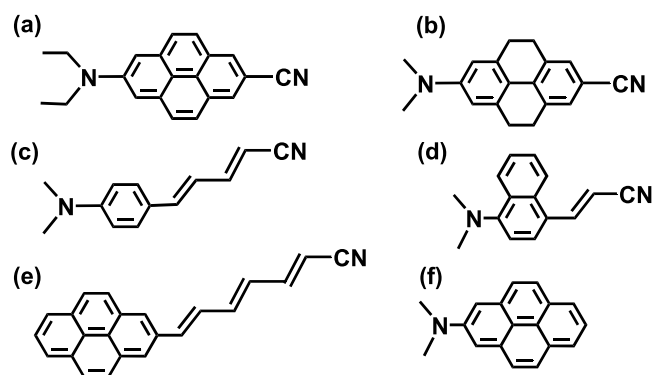
μ_e in the given equation are Planck's constant, the permittivity of vacuum, the velocity of light, the Onsagar cavity radius, the ground- and excited-state dipole moments, respectively. The increasing solvatochromism of the investigated $DANP_n$ molecules has been explained from the positive slope and the linear nature of the fitted straight line of the above-mentioned plot.

2.4. Generation of HOMO and LUMO Diagrams. The HOMO − 1, HOMO, LUMO, and LUMO + 1 frontier orbital diagrams were generated from the optimized checkpoint files using the Gauss View 5 software in the ACN solvent for all types of substituted pyrene molecules. To generate the molecular orbital diagrams, a surface isovalue of ±0.02 [e^{a0-3}]$^{1/2}$, the default setting in Gauss View 5, was used for all of the $DANP_n$ molecules, pyrene, and other 2/7-substituted supporting pyrene molecules.[19]

3. RESULTS AND DISCUSSION

We compared the results obtained using CAM-B3LYP and B3LYP functionals considering both the SS and the LR solvation approaches with the experimental results of the analogous ICT molecules (Scheme 4a,b)[21,26] and presented in

Scheme 4. Chemical Structure of Supporting and Other Reported ICT Molecules[a]

[a](a) Molecule used in expt 1, (b) molecule used in expt 2, (c) DMAPPDN, (d) DMANAN, (e) NP$_3$, and (f) DAP.

Figure 1. After comparison of the results (discussed in details within each subsection), it is clear that the CAM-B3LYP functional with the SS solvation method well supports the ICT process than the LR solvation approach and even better than the B3LYP functional. Therefore, below we discuss the results of the CAM-B3LYP functional with the SS and the LR methods considering the CPCM solvation model in the main article and other results are presented in the Supporting Information.

3.1. Ground- and Excited-State Geometries. Since the ICT phenomenon and corresponding spectral properties are directly related to the ground- and excited-state structural changes of the molecules, we focused on the structural changes of the studied molecules. The important parameters, which are observed to change during the excitation from the ground (optimized structure from step 1) to the first excited state (optimized structure from step 4), are presented in Table 1. All-trans conformation of the acceptor side chain of $DANP_n$ (n = 0−3) molecules provides the lowest-energy structure, as also reported from the crystal structure for such types of acceptor groups in D−π−A charge-transfer molecules.[15] We found that
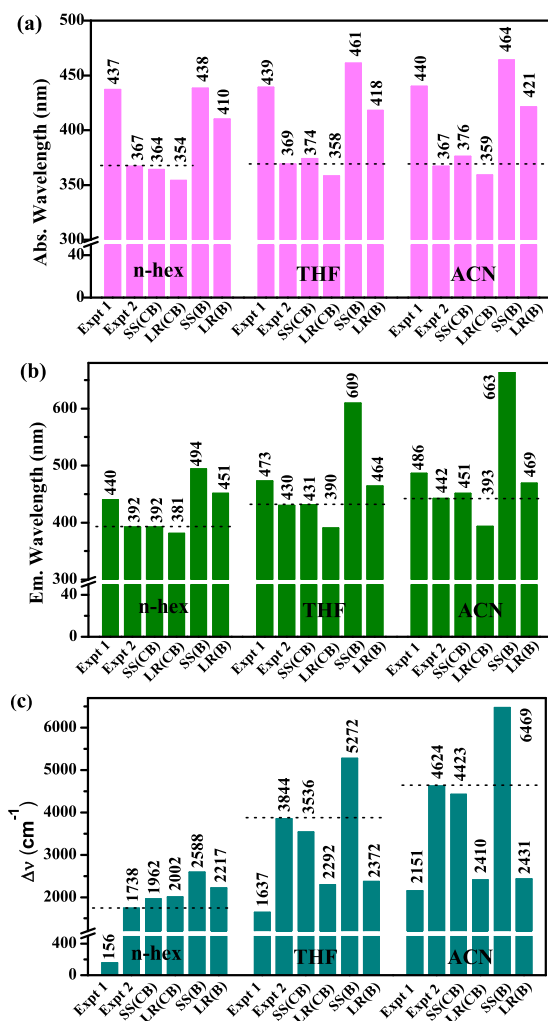
Figure 1. Plot of spectroscopic parameters obtained using different calculation methods for the DANP$_0$ molecule in n-hex, THF, and ACN solvents and experimentally reported results of two analogous ICT molecules. (a) Absorption, (b) fluorescence, and (c) Stokes' shifts are plotted against different methods. Expt 1 and expt 2 are the experimental results taken from refs [21], [26], respectively. SS and LR represent state-specific and linear-response solvations, respectively, CB and B within the parenthesis indicate the results using CAM-B3LYP and B3LYP functionals, respectively. The data shown in the n-hex solvent for expt 2 are taken from the cyclohexane solvent. The dotted lines are presented to easily compare the closeness of expt 2 and the computational results.

Table 1. Ground- and Excited-State-Optimized Parameters In Vacuo and Different Solvents[a]

molecules	parameters	Vac$_g$	Vac$_e$	ΔVac	THF$_g$	THF$_e$	ΔTHF	ACN$_g$	ACN$_e$	ΔACN	H$_2$O$_g$	H$_2$O$_e$	ΔH$_2$O
DANP$_0$	N$_2$–C$_{10}$	1.380	1.366	−0.014	1.374	1.355	−0.019	1.373	1.353	−0.020	1.373	1.352	−0.021
	C$_1$–N$_2$–C$_3$	118.2	118.4	0.2	118.3	117.2	−1.1	118.3	118.0	−0.3	118.3	116.3	−2.00
	C$_1$–N$_2$–C$_3$–C$_{10}$	161.6	179.9	18.3	162.6	180.0	17.4	162.7	180.0	17.3	162.7	180.0	17.3
	C$_1$–N$_2$–C$_3$–C$_{10}$–C$_{11}$	9.4	0.0	−9.4	9.0	6.5	−2.5	8.9	0.0	−8.9	8.9	0.0	0.0
DANP$_1$	N$_2$–C$_{10}$	1.381	1.368	−0.013	1.377	1.357	−0.02	1.376	1.354	−0.022	1.376	1.354	−0.022
	C$_1$–N$_2$–C$_3$	118.1	118.7	0.6	117.9	118.3	0.4	117.8	118.2	0.4	117.8	118.2	0.4
	C$_1$–N$_2$–C$_3$–C$_{10}$	160.5	180.0	19.5	159.9	180.0	20.1	159.9	179.9	20.0	159.9	179.9	20.0
	C$_1$–N$_2$–C$_3$–C$_{10}$–C$_{11}$	10.4	0.0	−10.4	10.7	0.0	−10.7	10.7	0.7	−10.0	10.7	0.6	−10.1
DANP$_2$	N$_2$–C$_{10}$	1.382	1.382	0	1.378	1.356	−0.022	1.378	1.354	−0.024	1.378	1.354	−0.024
	C$_1$–N$_2$–C$_3$	118.0	118.9	0.9	117.6	118.9	1.3	117.6	118.8	1.2	117.6	118.8	1.2
	C$_1$–N$_2$–C$_3$–C$_{10}$	159.5	179.9	20.4	158.4	180.0	21.6	158.4	179.9	21.5	158.4	180.0	21.6
	C$_1$–N$_2$–C$_3$–C$_{10}$–C$_{11}$	10.9	0.0	−10.9	11.5	0.0	−11.5	11.4	0.0	−11.4	11.4	0.0	−11.4
DANP$_3$	N$_2$–C$_{10}$	1.381	1.367	−0.014	1.379	1.36	−0.019	1.379	1.359	−0.02	1.379	1.358	−0.021
	C$_1$–N$_2$–C$_3$	117.5	119.2	1.7	117.5	119.1	1.6	117.5	119.0	1.5	117.5	119.1	1.6
	C$_1$–N$_2$–C$_3$–C$_{10}$	160.0	180.0	20.0	157.6	180.0	22.4	157.6	180.0	22.4	157.6	180.0	22.4
	C$_1$–N$_2$–C$_3$–C$_{10}$–C$_{11}$	10.7	0.0	−10.7	11.8	0.0	−11.8	11.9	0.1	−11.8	11.9	0.1	−11.8

[a]Where the subscript g and e denote the ground and excited states, respectively. Vac, THF, ACN, and H$_2$O represent the vacuo, tetrahydrofuran, acetonitrile, and water solvents, respectively. Δ represents the difference from the excited to ground state.

a number of parameters change significantly at the donor and acceptor sides, whereas no significant changes are observed within the pyrene ring. The data as shown in Table 1 show that the N$_2$–C$_{10}$ bond length (Scheme 5) is slightly shorter in the excited state by an amount of maximum 0.024 Å and this shortening increases with increasing solvent polarity (Table 1). The C$_1$–N$_2$–C$_3$ bond angle shows a change in the studied DANP$_n$ molecules. For DANP$_0$, this angle reduces by 0.3−2° with increasing solvent polarity, except in vacuum, where a small positive change is observed. For the other three DANP$_{n=1-3}$ molecules, with increasing the additional C═C− C bond on the donor side, this angle increases (Table 1 and Scheme 5), but this is almost independent on the polarity of the solvents. The C$_1$–N$_2$–C$_3$–C$_{10}$ dihedral angle also significantly increases from ground-state to excited-state by

Scheme 5. Atom Numbering of DANP$_n$ Molecules at the Ground-State Optimized Structures in the ACN Solvent
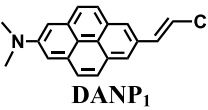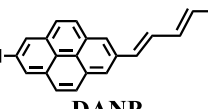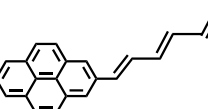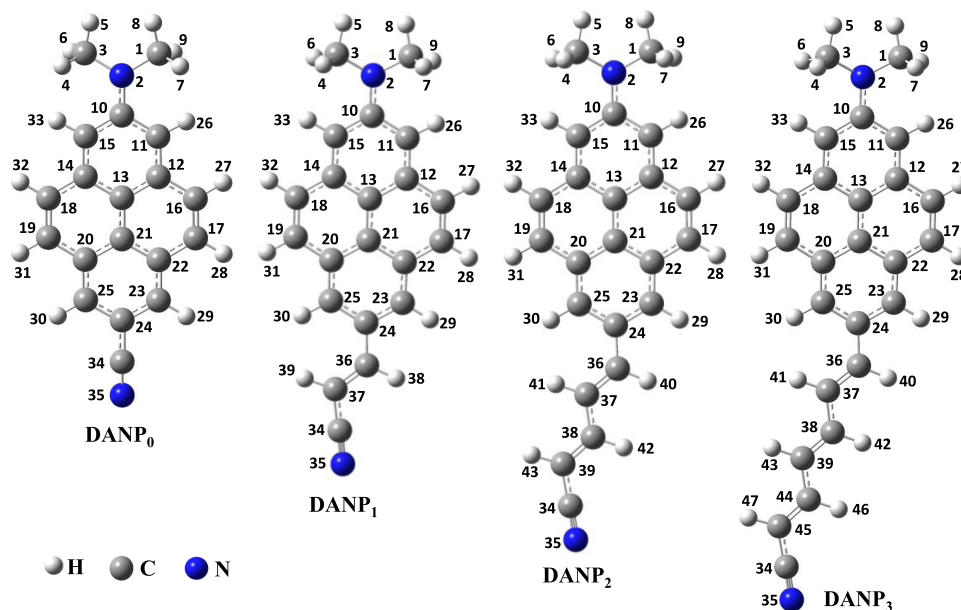

17.3 to 22.4° with increasing the value of $n = 0-3$. Another important dihedral angle $C_1-N_2-C_{10}-C_{11}$ is also found to decrease considerably by 8.9–11.8° to reach to the planer form except for the DANP$_0$ molecule in THF and H$_2$O solvents. Such types of dihedral angles between the donor and chromophore planes have already been observed for reported other planer ICT molecules.[21,46,47] The planarization of the D−π−A molecule in the excited state supports the possibility of more electronic delocalization from the donor to the acceptor group. This results in a higher dipolar character of the excited state. As the delocalization increases with increasing the number of the C═C−C bond in DANP$_n$ molecules, the C−C single bonds become shorten and C═C double bonds become elongated within the side chain.

3.2. Absorption Spectral Characteristic. As shown in Figure 1a, the absorption band positions in different solvents obtained from the CAM-B3LYP/SS-CPCM results are well-matched with the reported literature, here we mentioned it as experiment 2 (expt 2)[26] (Scheme 4b). We also compared the results with another literature, which reported an analogous ICT molecule in experiment 1 (expt 1).[21] The molecule DANP$_0$ shows the lowest-energy absorption band at 364 nm in n-hex (ca. expt 2 value 367 nm in cyclohexane); this band is originated from S$_0$ → S$_1$ electronic transition with $\varepsilon = 2872$ M^{-1} cm^{-1} (ca. experimental value 2800 M^{-1} cm^{-1} for the molecule in Scheme 4a)[21,26] and oscillator strength $f = 0.038$ (Table 2). The lowest-energy absorption band is slightly red-shifted to 376 nm in ACN and H$_2$O with $f = 0.036$ and 0.037, respectively. Such types of spectral shifts also reported in the literature for ICT molecules.[15,16,22] The f value suggests that the transition is of $\pi \to \pi^*$ nature. The results obtained using the B3LYP/SS-CPCM and LR-CPCM methods (Table S1) moderately correlate with expt 1 but fail to correlate with the results of absorption spectra from expt 2 (Figure 1a). Increasing the donor−acceptor distance of rest of the DANP$_n$ molecules ($n = 1-3$), the absorption band positions are gradually red-shifted from 368 to 377 nm in n-hex and 375 to 383 nm in ACN. The shift of the absorption maximum is reasonable as also observed in experimentally reported 2, 7-

disubstituted pyrene molecules.[19,21,28] A distinguishable shift of the absorption band position is observed between the DANP$_1$ and DANP$_2$ molecules (Table 2). When comparing the absorption maximum between n-hex and ACN solvents, a 12 nm difference is observed for DANP$_0$, whereas this difference is almost constant to 6−7 nm for the rest of the DANP$_{n=1-3}$ molecules. The oscillator strength value in polar protic and polar aprotic solvents is slightly less than that of the nonpolar solvent and the value gradually increases with increasing the value of n for DANP$_n$ molecules. A noticeable jump is observed for the DANP$_3$ molecule, where the lowest-energy S$_0$ → S$_1$ electronic transition is more intense than the other higher-level transitions, unlike for the DANP$_{n=0-2}$ molecules. The absorption band is independent of the hydrogen-bonding solvents for DANP$_{n=0-2}$ molecules, whereas an 8 nm blue shift is observed for the DANP$_3$ molecule (Table 2). Such type of blue-shifting of the absorption spectrum in hydrogen-bonding solvents is also reported for the D−π−A charge-transfer systems, like DMAPPDN[22] and DMANAN[13] (Scheme 4c,d). The light-harvesting property of the studied DANP$_n$ molecules gradually increases with increasing the value of n. DANP$_{0-2}$ molecules show low LHE property, which is 8, 10, and 28%, respectively, in the ACN solvent, whereas for DANP$_3$, it is 98%, which is relatively higher but comparable with other charge-transfer pyrene molecules.[28]

3.3. Steady-State Emission. The CAM-B3LYP/SS-CPCM results for emission spectra and Stokes' shift in n-hex, THF, and ACN solvents correlate well with expt 2 (Figure 1b,c), whereas the results obtained by B3LYP/SS-CPCM and LR-CPCM methods match less well. The fluorescence band positions for the S$_1$ → S$_0$ electronic transitions of the studied molecules in different polar aprotic and polar protic solvents with increasing polarity and hydrogen-bonding abilities are presented in Table 2. The DANP$_0$ molecule shows the fluorescence band maximum at 392 and 451 nm in n-hex and ACN solvents, respectively (ca. 392 nm in cyclohexane and 442 nm in ACN from expt 2), with a positive emission solvatochromism, 59 nm (2447 cm^{-1}), matched well with the experimentally reported values 50 and 46 nm for expt 2 and 1,

Table 2. Calculated Spectroscopic Parameters for Absorption and Fluorescence Processes[a]

ICT molecules	Solvent	λ_{abs} (nm) (S$_0$→S$_1$)	$\varepsilon \times 10^{-3}$ (M^{-1} cm^{-1})	f_{osc}	λ_{em} (nm) (S$_1$→S$_0$)	$\Delta\nu = \nu_a - \nu_f$ (cm^{-1})
DANP$_0$	Vacuo	350 (350)	1.59	0.037	375 (375)	1878 (1905)
	n-hex	364 (354)	2.87	0.038	392 (381)	1962 (2002)
	DOX	366 (355)	3.00	0.038	397 (383)	2122 (2059)
	CHCl$_3$	372 (357)	2.60	0.037	420 (388)	3055 (2238)
	THF	374 (358)	2.29	0.034	431 (390)	3536 (2292)
	ACN	376 (359)	1.93	0.036	451 (393)	4423 (2410)
	BuOH	376 (359)	2.15	0.035	444 (392)	4061 (2345)
	EtOH	376 (359)	2.00	0.034	448 (393)	4284 (2410)
	MeOH	375 (359)	1.88	0.034	450 (393)	4441 (2410)
	H$_2$O	376 (360)	1.88	0.037	454 (394)	4568 (2397)
DANP$_1$	Vacuo	358 (358)	3.98	0.045	383 (383)	1770 (1823)
	n-hex	368 (362)	11.50	0.047	394 (388)	1820 (1851)
	DOX	370 (363)	12.85	0.049	398 (389)	1917 (1841)
	CHCl$_3$	373 (364)	14.69	0.047	413 (393)	2568 (2027)
	THF	374 (365)	14.26	0.045	421 (395)	2948 (2081)
	ACN	375 (365)	13.73	0.048	434 (397)	3609 (2208)
	BuOH	375 (365)	14.77	0.046	429 (396)	3345 (2145)
	EtOH	375 (365)	14.02	0.044	432 (397)	3507 (2208)
	MeOH	375 (365)	13.34	0.044	434 (397)	3619 (2208)
	H$_2$O	375 (365)	13.54	0.045	436 (398)	3722 (2272)
DANP$_2$	Vacuo	361 (361)	27.22	0.118	386 (386)	1794 (1794)
	n-hex	369 (365)	54.32	0.134	396 (391)	1848 (1822)
	DOX	370 (365)	56.84	0.152	399 (392)	1964 (1887)
	CHCl$_3$	374 (366)	58.92	0.143	488 (453)	6246 (5247)
	THF	374 (367)	57.09	0.129	513 (463)	7245 (5650)
	ACN	375 (367)	54.50	0.146	553 (481)	8583 (6458)
	BuOH	375 (367)	57.17	0.134	540 (476)	8148 (6240)
	EtOH	375 (367)	55.38	0.124	548 (479)	8418 (6371)
	MeOH	374 (367)	53.52	0.126	553 (480)	8655 (6415)
	H$_2$O	375 (367)	53.76	0.118	560 (483)	8810 (6544)
DANP$_3$	Vacuo	364 (364)	76.99	1.850	423 (423)	3832 (3832)
	n-hex	377 (374)	95.43	1.926	457 (464)	4643 (5186)
	DOX	385 (376)	96.47	1.976	467 (473)	4561 (5454)
	CHCl$_3$	393 (377)	97.14	1.928	516 (509)	6065 (6879)
	THF	389 (377)	96.31	1.836	541 (524)	7223 (7441)
	ACN	383 (376)	95.01	1.926	585 (548)	9016 (8348)
	BuOH	390 (377)	96.29	1.866	571 (541)	8128 (8041)
	EtOH	384 (377)	95.40	1.806	579 (545)	8771 (8177)
	MeOH	381 (376)	94.60	1.816	584 (547)	9123 (8314)
	H$_2$O	382 (376)	94.77	1.850	592 (552)	9286 (8480)

[a]Where λ_{abs} and λ_{em} are the lowest-energy absorption and fluorescence wavelengths. ε, f_{osc}, and $\Delta\nu$ are the molar extinction coefficient, oscillator strength, and Stokes' shift, respectively. The ε values are for the LR method and the values are calculated using default bandwidth of absorption spectra, as provided by Gauss View 5. The Stokes' shifts are calculated for the ICT process. The values in parenthesis are calculated using CAM-B3LYP/LR-CPCM method.

respectively.[21,26] For other intermediate polar aprotic DOX, CHCl$_3$, and THF solvents, Stokes' shift ($\Delta\nu$) gradually increases with increasing polarity of the solvents. 2447 cm^{-1} positive emission solvatochromism supports a weak charge transfer as reported for an analogous molecule.[21] The spectral data obtained using the B3LYP/SS-CPCM and LR-CPCM methods correlate less with the experimental data in n-hex, THF, and ACN solvents, as presented in Table S1. The B3LYP functional overestimates the fluorescence band position for the DANP$_0$ molecule. The fluorescence band is slightly red-shifted comparatively in more polar and hydrogen-bonding water solvents and appears at 454 nm when the CAM-B3LYP/SS-CPCM method is used. Overall, as increasing the solvent

hydrogen-bonding character with the polarity, the fluorescence band is 10 nm red-shifted from BuOH to water (Table 2). Addition of an extra C=C−C moiety to the DANP$_0$ molecule generates DANP$_1$. The fluorescence band of DANP$_1$ in n-hex and ACN solvents appears at 394 and 434 nm, respectively, with the 3609 cm^{-1} Stokes' shift in the ACN solvent. Similarly, DANP$_2$ and DANP$_3$ show a more red-shifted fluorescence band in ACN at 553 ($\Delta\nu$ = 8583 cm^{-1}) and 585 nm ($\Delta\nu$ = 9016 cm^{-1}) in the n-hex solvent at 396 and 457 nm, respectively. The fluorescence band in water appears at 560 and 592 nm for DANP$_2$ and DANP$_3$ molecules, respectively (Table 2). Among all of the studied molecules, DANP$_3$ shows the highest Stokes' shift 9286 cm^{-1} in water. Such type of the

huge Stokes' shift is also experimentally reported for D−π−A pyrene and other charge-transfer systems (Scheme 4c,d).[13,16,22] A maximum 21 nm red-shift is observed for the $DANP_3$ molecule in hydrogen-bonding solvents. Overall, it is clear that the excited states of $DANP_n$ molecules are more polar in nature compared to the ground state. This polar character gradually increases and stabilizes by the more polar solvents with increasing the value of n in $DANP_n$ molecules. As a result, we see more red-shifted fluorescence with the larger Stokes' shift (Table 2).

3.4. Excited-State Polarity and the Charge-Transfer Process.
The change of the dipole moment of $DANP_n$ molecules due to electronic transition from the ground to the excited state and the stability of the polar excited state in different polar media through solvation are main evidence of the generation of the ICT state. Therefore, the dipole moments of the ground- and excited-state equilibrium geometries in vacuum, n-hex, ACN, and water solvents are estimated and summarized in Table 3. Dipole moments for

Table 3. Ground and Excited Equilibria State Dipole Moments of the ICT Molecules In Vacuo and Different Solvents[a]

ICT molecules	solvents	μ_g	μ_e	$\Delta\mu$
$DANP_0$	vacuo	8.68	9.05	0.37
	n-hex	9.63	10.12	0.49
	ACN	11.07	11.75	0.68
	H_2O	11.12	11.81	0.69
$DANP_1$	vacuo	9.30	9.79	0.49
	n-hex	10.16	10.80	0.64
	ACN	11.34	12.24	0.90
	H_2O	11.38	12.29	0.91
$DANP_2$	vacuo	9.77	10.38	0.61
	n-hex	10.61	11.44	0.83
	ACN	11.73	15.53	3.80
	H_2O	11.77	15.64	3.87
$DANP_3$	vacuo	10.18	12.04	1.86
	n-hex	11.05	13.75	2.70
	ACN	12.14	16.82	4.68
	H_2O	12.18	16.96	4.78

[a]where μ_g and μ_e are the ground- and excited-state dipole moments and $\Delta\mu$ is the dipole moment difference ($\mu_e - \mu_g$).

other states in different solvents, as depicted in Scheme 3, are presented in Table S2. $DANP_0$ shows the ground-state dipole moment 8.68 Debye in a vacuum and 11.07 Debye in the ACN solvent, which are also comparable to the D−π−−A types of ICT molecules containing −CN as an acceptor, −NMe$_2$ as a donor, and different chromophores.[13,14] The ground-state dipole moments are not much different as increasing the value of n for the $DANP_n$ molecules and the values are observed to change almost within 1 Debye. Whereas, the excited-state dipole moment in the more polar water solvent is observed to increase approximately 5 Debye. Also, the excited-state dipole moment of the $DANP_3$ molecule in water and ACN solvents is almost 4.7 Debye larger than the ground-state geometry. The dipole moment differences of other nonequilibria states are ∼ 4 times more than the equilibria states (Table S2). The dipole moment difference between nonequilibrium and equilibrium states suggests the extent of stabilization of the ICT state through the solvation. Overall, the higher dipole moment of $DANP_n$ molecules in the excited state and the increasing dipole

moment difference between ground and excited states with increasing the value of n as well as solvent polarity well supports the existence of the polar excited state. Such types of the dipole moment difference from the ground to the excited state are possible due to redistribution of the charge from the donor to the acceptor after electronic excitation. This clearly suggests the formation of the ICT state for $DANP_n$ molecules.

For confirming the evidence of the charge-transfer process, we calculated Stokes' shift of $DANP_n$ molecules in nonpolar n-hex and different polar aprotic solvents with gradually increasing polarity and plotted the Lippart−Mataga relation (eq 5) of the solvent polarity parameter (Δf) against Stokes' shift ($\Delta\nu$ cm^{-1}).[45] As shown in Figure 2a, the plot shows linearity with the correlation coefficient, $R = 0.9987$. The rest of the $DANP_{n=1-3}$ molecules also show clear linear relationship with $R = 0.9975, 0.9814, 0.9879$, respectively (Figure 2b−d). However, in the case of polar protic solvents like BuOH, EtOH, MeOH, and water, a deviation from linearity are observed in the Lippert−Mataga plot, which indicates that hydrogen-bonding solvents have different types of influence on the charge-transfer state of the studied molecules. To further examine the different effects of polar protic and aprotic solvents on the charge-transfer state, we used the Reichard $E_T(30)$ parameter and plotted against Stokes' shift.[48] The $E_T(30)$ plots in Figure 3a−d clearly show two different straight lines with different slopes for the $DANP_n$ molecules, one for the polar protic and another for the polar aprotic solvents. In polar aprotic solvents only dipolar interaction is present, whereas in polar protic solvents both the dipolar as well as the hydrogen-bonding interactions are present to stabilize the charge-transfer state. To get further evidence of the dependence of the charge-transfer emission on the hydrogen-bonding solvents, we plotted the emission band maximum (ν_f cm^{-1}) against hydrogen-bonding strength (α) of different hydrogen-bonding solvents for the studied molecules.[23,49] The results in Figure 4a−d show linear dependence with the satisfactory linear fitting of the data points. These plots indicate that hydrogen-bonding solvents stabilize the charge-transfer state through hydrogen-bonding interaction in a different fashion in addition to the dipolar interaction.[22] Although, the effect of hydrogen-bonding solvents coincidentally matched with the experimental trend of other ICT molecules, these types of calculations did not consider explicit solvent model. To further check among the donor and acceptor which group is more important to the formation of the charge-transfer state, we carried out calculations in n-hex and ACN solvents for the NP$_3$ molecule ($DANP_3$ without the −NMe$_2$ group) and 2-N,N-dimethylamino pyrene (DAP), the molecule without the acceptor (Scheme 4e,f). The results are presented in Table S3. Although the DAP molecule shows more solvent polarity-dependent Stokes' shifted emission than NP$_3$, both the molecules did not show any strong solvent polarity dependency as observed for the $DANP_3$ molecule. Therefore, it is also clear that for the efficient charge-transfer process, the appropriate donor and acceptor groups have to be attached to the pyrene chromophore within the D−π−A system.

3.5. Analysis of Molecular Orbital Diagrams.
To further extract the evidence of the formation of the charge-transfer state and it's dependence on the D−A distance, we generated the molecular orbital (MO) diagrams from the optimized structure of $DANP_n$ molecules in the ACN solvent (Figure 5). Comparing with the earlier reported molecular orbital diagrams of the parent unsubstituted pyrene mole-
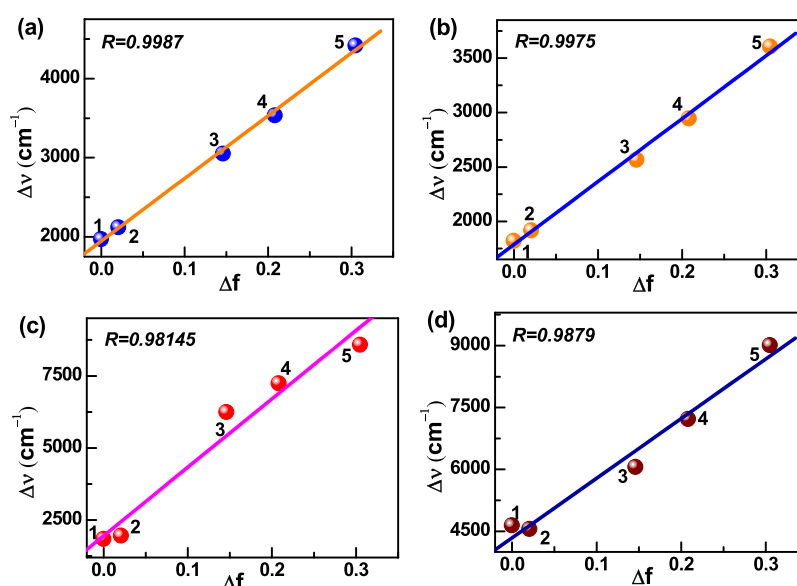
Figure 2. Plot of Stokes' shift ($\Delta\nu$) against the solvent polarity parameter (Δf), 1 → 5: n-hex, DOX, $CHCl_3$, THF, and ACN solvents for (a) $DANP_0$, (b) $DANP_1$, (c) $DANP_2$, and (d) $DANP_3$ molecules.

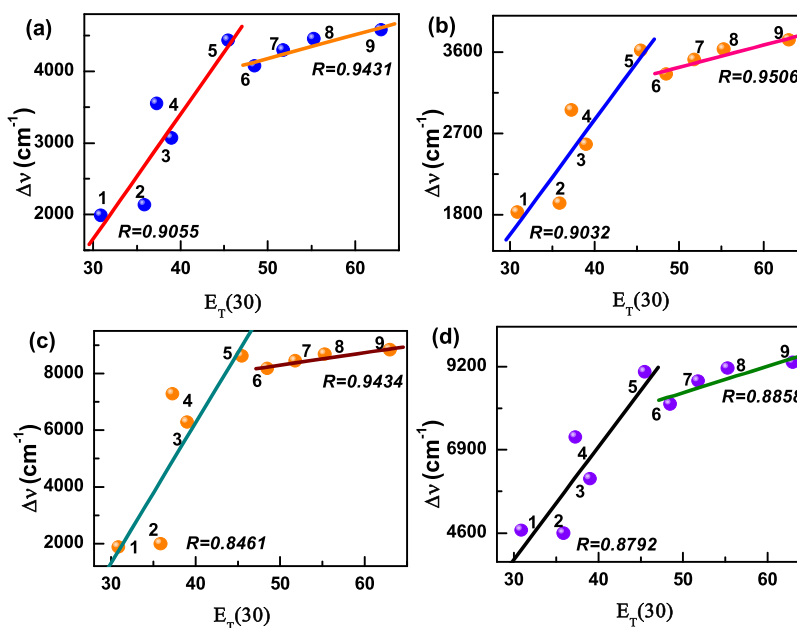**Figure 3.** Plot of Stokes' shift ($\Delta\nu$) against the Reichardt solvent polarity parameter, $E_T(30)$. 1 → 5 for nonpolar and polar aprotic solvents: n-hex, DOX, $CHCl_3$, THF, and ACN; 6 → 9 for hydrogen-bonding solvents: BuOH, EtOH, MeOH, and H_2O for (a) $DANP_0$, (b) $DANP_1$, (c) $DANP_2$, and (d) $DANP_3$ molecules.

cule,[19] we mainly focused on the HOMO − 1, HOMO, LUMO, and LUMO + 1 diagrams for the studied molecules. As shown in Figure 5, due to D−A 2,7-disubstitution to the parent pyrene molecule, the HOMO and HOMO − 1 orbitals shuffle their energy order with respect to unsubstituted pyrene (Figure S1).[19,30] In addition to that, increasing the length of the acceptor chain, the LUMO and LUMO + 1 orbitals interchange their energy order from the $DANP_0$ to $DANP_1$ molecule and rest of the $DANP_{n=2−3}$ molecules follow the MO energy order like $DANP_1$. Such type of LUMO and LUMO + 1 energy order shuffling is also observed by Merz et al. for other D−π−A-substituted pyrene molecules.[19,30] The orbital energy order shuffling reflects better optical and redox properties of these molecules as also reported for other

substituted pyrene molecules.[19] The HOMO of $DANP_n$ molecules is mainly localized on the −NMe_2 group and pyrene ring, whereas a lesser extent on the acceptor side chain and this trend is gradually more prominent as increasing the value of n in $DANP_n$ molecules. Gradually increasing the length of the acceptor side chain, the LUMO (LUMO + 1 for $DANP_0$) is gradually found to localize more on the acceptor side chain and to a lesser extent on the donor and chromophore groups. Therefore, the HOMO to LUMO electronic transition creates $DANP_n$ molecules of more dipolar nature. The less charge-transfer possibility of the $DANP_0$ molecule also may be explained when comparing the LUMO + 1 of $DANP_0$ with the LUMO of the rest of the molecules.[14,28,30] The more electron density on the N atom
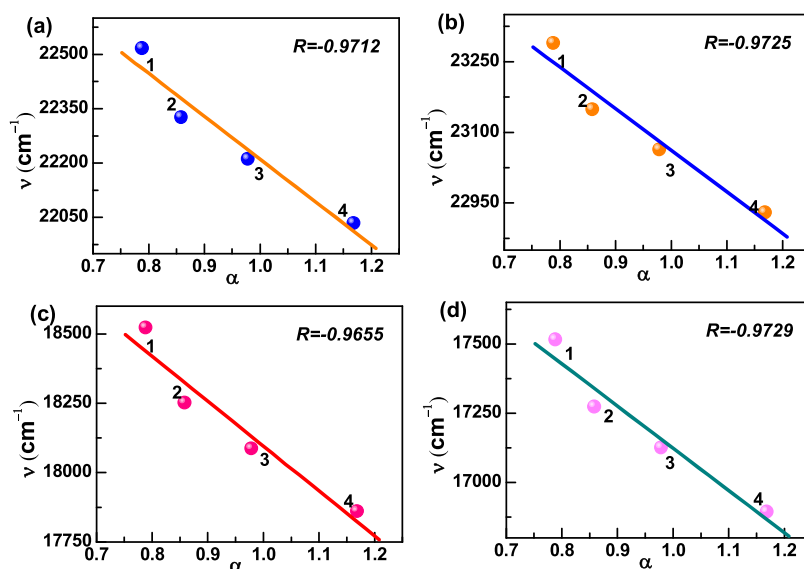
Figure 4. Plot of the fluorescence band maximum (ν) against the solvent hydrogen-bonding parameter (α), $1 \rightarrow 4$: BuOH, EtOH, MeOH, and H_2O for (a) $DANP_0$, (b) $DANP_1$, (c) $DANP_2$, and (d) $DANP_3$ molecules.
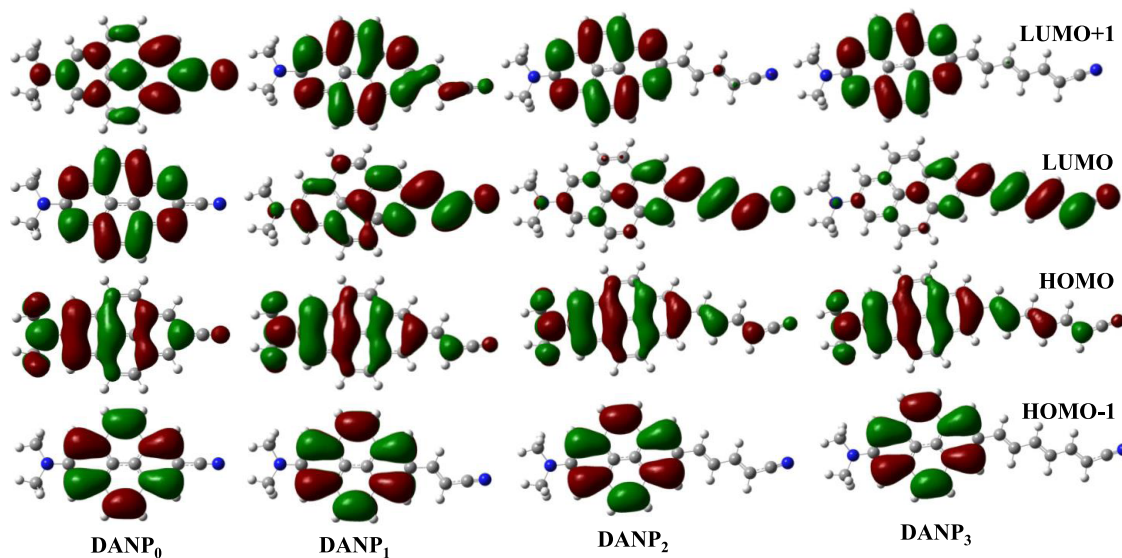

Figure 5. Molecular orbital diagrams of $DANP_n$ molecules in the ACN solvent.

of the $-NMe_2$ group and pyrene ring remains for $DANP_0$ (LUMO + 1), whereas it gradually decreases and shifts to the acceptor side chain through the pyrene moiety for $DANP_{n=1-3}$ molecules (LUMO). To check the involvement of the donor and acceptor groups to the formation of the charge-transfer state, we also generated the MO diagrams of DAP and NP_3 molecules (Figure S1). The HOMO and HOMO − 1 of DAP show the energy order shuffling in comparison to the MO of the unsubstituted pyrene. On the other hand, we see a similar situation between the LUMO and LUMO + 1 of NP_3. When both the donor and acceptor groups are attached to the pyrene chromophore, i.e., $DANP_3$ molecule, the nature of the HOMO−LUMO and the energy gap between them are observed to change, which may prompt the electronic transition and the formation of the ICT state.

3.6. Donor−Acceptor Distance-Dependent ICT Process. To investigate the D−A distance dependency on the ICT process, we compared the calculated dipole moment,

fluorescence band position, Stokes' shift, etc. as a function of the change of D−A distance, i.e., the number of C═C−C moieties, which is denoted by n for $DANP_n$ molecules. The presented data in Tables 2, 3 and S2, S3 clearly support that there are distinct changes in the above-mentioned parameters, which are responsible for the ICT phenomenon. Figure 6a shows the plot of the fluorescence band maxima against the change of D−A distance (n of $DANP_n$ molecules) in n-hex, THF, ACN, and H_2O solvents. The data support a linear relationship between the fluorescence band maximum in different polar solvents and increased D−A distance. It is clear that with increasing the value of n, the emissive species is more stabilized in polar solvents, which is clear from the positive slope of the above plot in different solvents of increasing polarity. Figure 6b reveals that Stokes' shift of the $DANP_n$ molecules in the ACN solvent increases linearly ($R = 0.8687$) as changing the D−A distance. The dipole moment difference between equilibrium ground and excited states in
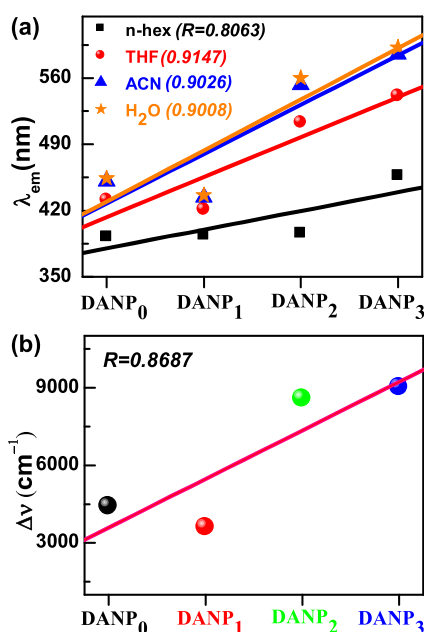
Figure 6. (a) Plot of the fluorescence band position in different solvents against ICT molecules of different donor−acceptor distances. (b) Stokes' shift in the ACN solvent vs ICT molecules of different donor−acceptor distances. The donor−acceptor distance here is represented by the number of the C≡C−C moiety within the chromophore and acceptor.

ACN solvent also increases from 0.68 to 4.68 Debye as increasing the value of n (Table 3). On the other hand, on increasing the D−A distance, the light-harvesting efficiency (LHE) in the ACN solvent increases from 8 to 98% for $n = 0-3$ of $DANP_n$ molecules. As a whole, the emission solvatochromism increases with increasing the donor−acceptor distance and we see the highest emission solvatochromism 9286 cm^{-1} for the $DANP_3$ molecule in water. The MO energy order as well as MO distribution both change as the donor−acceptor distance increases, which also influences the ICT phenomenon.

4. CONCLUSIONS

We have successfully designed and established the ICT phenomenon of a set of donor−acceptor-substituted pyrene dye molecules by quantum chemical calculations and reported the D−A distance-dependent ICT process. The computational results obtained from the CAM-B3LYP/SS-CPCM method better agree with the experimental results than other methods to support the ICT phenomenon. Solvatochromism, structural and dipolar changes between the ground and the excited states are well evidence for the ICT process, which passes through the planer ICT mechanism. Polar aprotic solvents have different influences on the stability of the ICT state than the polar aprotic solvents. The increase of the donor−acceptor distance maintains a linear trend with the properties of emission maxima, dipole moment difference between ground and excited states, Stokes' shift, oscillator strength, and light-harvesting properties. Increasing the oscillator strength value as a function of the D−A distance well supports the enhanced optical properties and quantum yield. In the future, this work will help and motivate to further synthesize pyrene ICT molecules experimentally to use their physical and light-harvesting properties. Finally, it is evident that for the

enhanced charge-transfer phenomenon and light-harvesting properties of pyrene dye molecules, D−π−A moieties are essential and require adequate distance between the donor and acceptor.

■ ASSOCIATED CONTENT

Ⓢi Supporting Information

The Supporting Information is available free of charge at https://pubs.acs.org/doi/10.1021/acsomega.0c00265.

Calculated spectroscopic parameters for the $DANP_0$ molecule in n-hex, THF, and ACN solvents using B3LYP functional and different methods (Table S1), dipole moments of different ground- and excited-state structures in different solvents (Table S2), calculated spectroscopic parameters for DAP and NP_3 molecules in n-hex and ACN solvents (Table S3), MO diagrams of pyrene, DAP, and NP_3 molecules in the ACN solvent (Figure S1) (PDF)

■ AUTHOR INFORMATION

Corresponding Author

Sankar Jana − *School of Biology, Biomedical Science Research Complex, University of St Andrews, North Haugh, St Andrews, Fife KY16 9ST, United Kingdom;* ⓞ orcid.org/0000-0003-2274-9082; Phone: +44 (0)1334 463401; Email: sankjana@gmail.com; Fax: +44 (0)1334 462595

Author

Dipanwita Jana − *Bishnupada Sarkar College of Education, Gourhati, Arambagh, Hooghly, West Bengal 712613, India*

Complete contact information is available at:
https://pubs.acs.org/10.1021/acsomega.0c00265

Notes

The authors declare no competing financial interest.

■ REFERENCES

(1) Grabowski, Z. R.; Rotkiewicz, K.; Rettig, W. Structural Changes Accompanying Intramolecular Electron Transfer: Focus on Twisted Intramolecular Charge-Transfer States and Structures. *Chem. Rev.* **2003**, *103*, 3899−4032.

(2) Lippert, E.; Lüder, W.; Moll, F.; Nägele, W.; Boos, H.; Prigge, H.; Seibold-Blankenstein, I. Umwandlung von Elektronenanregungsenergie. *Angew. Chem., Int. Ed.* **1961**, *73*, 695−706.

(3) Lai, R. Y.; Fabrizio, E. F.; Lu, L.; Jenekhe, S. A.; Bard, A. J. Synthesis, Cyclic Voltammetric Studies, and Electrogenerated Chemiluminescence of a New Donor Acceptor Molecule: 3,7-[Bis[4-phenyl-2-quinolyl]]-10-methylphenothiazine. *J. Am. Chem. Soc.* **2001**, *123*, 9112−9118.

(4) Yang, Y.; Zou, J.; Rong, H.; Qian, G. D.; Wang, Z. Y.; Wang, M. Q. Influence of various coumarin dyes on the laser performance of laser dyes co-doped into ORMOSILs. *Appl. Phys. B* **2007**, *86*, 309−313.

(5) Grimm, J. B.; English, B. P.; Chen, J.; Slaughter, J. P.; Zhang, Z.; Revyakin, A.; Patel, R.; Macklin, J. J.; Normanno, D.; Singer, R. H.; Lionnet, T.; Lavis, L. D. A general method to improve fluorophores for live-cell and single-molecule microscopy. *Nat. Methods* **2015**, *12*, 244−250.

(6) Hara, K.; Tachibana, Y.; Ohga, Y.; Shinpo, A.; Suga, S.; Sayama, K.; Sugihara, H.; Arakawa, H. Dye-sensitized nanocrystalline TiO2 solar cells based on novel coumarin dyes. *Sol. Energy Mater. Sol. Cells* **2003**, *77*, 89−103.

(7) Wang, Z.-S.; Cui, Y.; Hara, K.; Dan-oh, Y.; Kasada, C.; Shinpo, A. A High-Light-Harvesting-Efficiency Coumarin Dye for Stable Dye-Sensitized Solar Cells. *Adv. Mater.* **2007**, *19*, 1138−1141.

(8) Jana, S.; Dalapati, S.; Ghosh, S.; Guchhait, N. Potential charge transfer probe induced conformational changes of model plasma protein human serum albumin: Spectroscopic, molecular docking, and molecular dynamics simulation study. *Biopolymers* **2012**, *97*, 766−777.

(9) Park, S.; Steen, C. J.; Lyska, D.; Fischer, A. L.; Endelman, B.; Iwai, M.; Niyogi, K. K.; Fleming, G. R. Chlorophyll−carotenoid excitation energy transfer and charge transfer in Nannochloropsis oceanica for the regulation of photosynthesis. *Proc. Natl. Acad. Sci. U.S.A.* **2019**, *116*, 3385−3390.

(10) Jana, S.; Du, T.; Nagao, R.; Noguchi, T.; Shibata, Y. Redox-state dependent blinking of single photosystem I trimers at around liquid-nitrogen temperature. *Biochim. Biophys. Acta, Bioenerg.* **2018**, *1860*, 30−40.

(11) Jana, S.; Ghosh, S.; Dalapati, S.; Guchhait, N. Exploring structural change of protein bovine serum albumin by external perturbation using extrinsic fluorescence probe: spectroscopic measurement, molecular docking and molecular dynamics simulation. *Photochem. Photobiol. Sci.* **2012**, *11*, 323−332.

(12) Jana, S.; Dalapati, S.; Ghosh, S.; Guchhait, N. Study of microheterogeneous environment of protein Human Serum Albumin by an extrinsic fluorescent reporter: A spectroscopic study in combination with Molecular Docking and Molecular Dynamics Simulation. *J. Photochem. Photobiol., B* **2012**, *112*, 48−58.

(13) Singh, R. B.; Mahanta, S.; Kar, S.; Guchhait, N. Spectroscopic and theoretical evidence for the photoinduced twisted intramolecular charge transfer state formation in N,N-dimethylaminonaphthyl-(acrylo)-nitrile. *J. Lumin.* **2008**, *128*, 1421−1430.

(14) Muralidharan, S.; Sinha, H. K.; Yates, K. Conformational effects on charge-transfer properties in selected 9,10-disubstituted anthracene derivatives: ground- and excited-state dipole moments. *J. Phys. Chem. A* **1991**, *95*, 8517−8520.

(15) Jana, S.; Dalapati, S.; Ghosh, S.; Guchhait, N. Excited state intramolecular charge transfer process in 5-(4-dimethylamino-phenyl)-penta-2,4-dienoic acid ethyl ester and effect of acceptor functional groups. *J. Photochem. Photobiol., A* **2013**, *261*, 31−40.

(16) Jana, S.; Ghosh, S.; Dalapati, S.; Kar, S.; Guchhait, N. Photoinduced intramolecular charge transfer phenomena in 5-(4-dimethylamino-phenyl)-penta-2,4-dienoic acid. *Spectrochim. Acta, Part A* **2011**, *78*, 463−468.

(17) Ghosh, S.; Jana, S.; Nath, D.; Guchhait, N. Fluorescent Probing of Protein Bovine Serum Albumin Stability and Denaturation Using Polarity Sensitive Spectral Response of a Charge Transfer Probe. *J. Fluoresc.* **2011**, *21*, 365−374.

(18) Jana, S.; Dalapati, S.; Ghosh, S.; Guchhait, N. Binding interaction between plasma protein bovine serum albumin and flexible charge transfer fluorophore: A spectroscopic study in combination with molecular docking and molecular dynamics simulation. *J. Photochem. Photobiol., A* **2012**, *231*, 19−27.

(19) Merz, J.; Fink, J.; Friedrich, A.; Krummenacher, I.; Al Mamari, H. H.; Lorenzen, S.; Haehnel, M.; Eichhorn, A.; Moos, M.; Holzapfel, M.; Braunschweig, H.; Lambert, C.; Steffen, A.; Ji, L.; Marder, T. B. Pyrene Molecular Orbital Shuffle—Controlling Excited State and Redox Properties by Changing the Nature of the Frontier Orbitals. *Chem. Eur. J.* **2017**, *23*, 13164−13180.

(20) Niko, Y.; Sasaki, S.; Narushima, K.; Sharma, D. K.; Vacha, M.; Konishi, G.-i. 1-, 3-, 6-, and 8-Tetrasubstituted Asymmetric Pyrene Derivatives with Electron Donors and Acceptors: High Photostability and Regioisomer-Specific Photophysical Properties. *J. Org. Chem.* **2015**, *80*, 10794−10805.

(21) Ji, L.; Lorbach, A.; Edkins, R. M.; Marder, T. B. Synthesis and Photophysics of a 2,7-Disubstituted Donor-Acceptor Pyrene De-

(22) Jana, S.; Dalapati, S.; Ghosh, S.; Kar, S.; Guchhait, N. Excited State Charge Transfer reaction with dual emission from 5-(4-dimethylamino-phenyl)-penta-2,4-dienenitrile: Spectral measurement and theoretical density functional theory calculation. *J. Mol. Struct.* **2011**, *998*, 136−143.

(23) Jana, S.; Dalapati, S.; Guchhait, N. Excited State Intramolecular Charge Transfer Suppressed Proton Transfer Process in 4-(Diethylamino)-2-hydroxybenzaldehyde. *J. Phys. Chem. A* **2013**, *117*, 4367−4376.

(24) Nandy, R.; Sankararaman, S. Donor-acceptor substituted phenylethynyltriphenylenes − excited state intramolecular charge transfer, solvatochromic absorption and fluorescence emission. *Beilstein J. Org. Chem.* **2010**, *6*, 992−1001.

(25) Ferreira, D. P.; Conceição, D. S.; Prostota, Y.; Santos, P. F.; Ferreira, L. F. V. Fluorescent "rhodamine-like" hemicyanines derived from the 6-(N,N-diethylamino)-1,2,3,4-tetrahydroxanthylium system. *Dyes Pigm.* **2015**, *112*, 73−80.

(26) Sumalekshmy, S.; Gopidas, K. R. Photoinduced Intramolecular Charge Transfer in Donor−Acceptor Substituted Tetrahydropyrenes. *J. Phys. Chem. B* **2004**, *108*, 3705−3712.

(27) Pedone, A. Role of Solvent on Charge Transfer in 7-Aminocoumarin Dyes: New Hints from TD-CAM-B3LYP and State Specific PCM Calculations. *J. Chem. Theory Comput.* **2013**, *9*, 4087−4096.

(28) Kathiravan, A.; Panneerselvam, M.; Sundaravel, K.; Pavithra, N.; Srinivasan, V.; Anandan, S.; Jaccob, M. Unravelling the effect of anchoring groups on the ground and excited state properties of pyrene using computational and spectroscopic methods. *Phys. Chem. Chem. Phys.* **2016**, *18*, 13332−13345.

(29) Sun, F.; Jin, R. DFT and TD-DFT study on the optical and electronic properties of derivatives of 1,4-bis(2-substituted-1,3,4-oxadiazole)benzene. *Arabian J. Chem.* **2017**, *10*, S2988−S2993.

(30) Crawford, A. G.; Dwyer, A. D.; Liu, Z.; Steffen, A.; Beeby, A.; Pålsson, L.-O.; Tozer, D. J.; Marder, T. B. Experimental and Theoretical Studies of the Photophysical Properties of 2- and 2,7-Functionalized Pyrene Derivatives. *J. Am. Chem. Soc.* **2011**, *133*, 13349−13362.

(31) Zhou, Y.; Yang, Q.; Cuan, J.; Wang, Y.; Gan, N.; Cao, Y.; Li, T. A pyrene-involved luminescent MOF for monitoring 1-hydroxypyrene, a biomarker for human intoxication of PAH carcinogens. *Analyst* **2018**, *143*, 3628−3634.

(32) Ifegwu, C.; Osunjaye, K.; Fashogbon, F.; Oke, K.; Adeniyi, A.; Anyakora, C. Urinary 1-Hydroxypyrene as a Biomarker to Carcinogenic Polycyclic Aromatic Hydrocarbon Exposure. *Biomarkers Cancer* **2012**, *4*, No. BIC.S10065.

(33) Masuko, M.; Ohuchi, S.; Sode, K.; Ohtani, H.; Shimadzu, A. Fluorescence resonance energy transfer from pyrene to perylene labels for nucleic acid hybridization assays under homogeneous solution conditions. *Nucleic Acids Res.* **2000**, *28*, e34−00.

(34) Conlon, P.; Yang, C. J.; Wu, Y.; Chen, Y.; Martinez, K.; Kim, Y.; Stevens, N.; Marti, A. A.; Jockusch, S.; Turro, N. J.; Tan, W. Pyrene Excimer Signaling Molecular Beacons for Probing Nucleic Acids. *J. Am. Chem. Soc.* **2008**, *130*, 336−342.

(35) Casas-Solvas, J. M.; Howgego, J. D.; Davis, A. P. Synthesis of substituted pyrenes by indirect methods. *Org. Biomol. Chem.* **2014**, *12*, 212−232.

(36) Improta, R.; Barone, V.; Scalmani, G.; Frisch, M. J. A state-specific polarizable continuum model time dependent density functional theory method for excited state calculations in solution. *J. Chem. Phys.* **2006**, *125*, No. 054103.

(37) Adamo, C.; Jacquemin, D. The calculations of excited-state properties with Time-Dependent Density Functional Theory. *Chem. Soc. Rev.* **2013**, *42*, 845−856.

(38) Krawczyk, P. Time-dependent density functional theory calculations of the solvatochromism of some azo sulfonamide fluorochromes. *J. Mol. Model.* **2015**, *21*, 118.

(39) Takano, Y.; Houk, K. N. Benchmarking the Conductor-like Polarizable Continuum Model (CPCM) for Aqueous Solvation Free Energies of Neutral and Ionic Organic Molecules. *J. Chem. Theory Comput.* **2005**, *1*, 70−77.

(40) Barone, V.; Cossi, M. Quantum Calculation of Molecular Energies and Energy Gradients in Solution by a Conductor Solvent Model. *J. Phys. Chem. A* **1998**, *102*, 1995−2001.

(41) Improta, R.; Scalmani, G.; Frisch, M. J.; Barone, V. Toward effective and reliable fluorescence energies in solution by a new state specific polarizable continuum model time dependent density functional theory approach. *J. Chem. Phys.* **2007**, *127*, No. 074504.

(42) Jana, S.; Dalapati, S.; Guchhait, N. Functional group induced excited state intramolecular proton transfer process in 4-amino-2-methylsulfanyl-pyrimidine-5-carboxylic acid ethyl ester: a combined spectroscopic and density functional theory study. *Photochem. Photobiol. Sci.* **2013**, *12*, 1636−1648.

(43) Yanai, T.; Tew, D. P.; Handy, N. C. A new hybrid exchange−correlation functional using the Coulomb-attenuating method (CAM-B3LYP). *Chem. Phys. Lett.* **2004**, *393*, 51−57.

(44) Frisch, M.; Trucks, G.; Schlegel, H.; Scuseria, G.; Robb, M.; Cheeseman, J.; Scalmani, G.; Barone, V.; Mennucci, B.; Petersson, G.; Nakatsuji, H.; Caricato, M.; Li, X.; Hratchian, H.; Izmaylov, A.; Bloino, J.; Zheng, G.; Sonnenberg, J.; Hada, M.; Fox, D. *Gaussian 09*, revision D.01; Gaussian Inc.: Wallingford, CT, 2009.

(45) Mataga, N.; Chosrowjan, H.; Taniguchi, S. Ultrafast charge transfer in excited electronic states and investigations into fundamental problems of exciplex chemistry: Our early studies and recent developments. *J. Photochem. Photobiol., C* **2005**, *6*, 37−79.

(46) Zachariasse, K. A.; Grobys, M.; von der Haar, T.; Hebecker, A.; Il'ichev, Y. V.; Jiang, Y. B.; Morawski, O.; Kühnle, W. Intramolecular charge transfer in the excited state. Kinetics and configurational changes. *J. Photochem. Photobiol., A* **1996**, *102*, 59−70.

(47) Liu, X.; Cole, J. M.; Xu, Z. Substantial Intramolecular Charge Transfer Induces Long Emission Wavelengths and Mega Stokes Shifts in 6-Aminocoumarins. *J. Phys. Chem. C* **2017**, *121*, 13274−13279.

(48) Reichardt, C. Solvatochromic Dyes as Solvent Polarity Indicators. *Chem. Rev.* **1994**, *94*, 2319−2358.

(49) Jana, S.; Dalapati, S.; Guchhait, N. Proton Transfer Assisted Charge Transfer Phenomena in Photochromic Schiff Bases and Effect of -NEt$_2$ Groups to the Anil Schiff Bases. *J. Phys. Chem. A* **2012**, *116*, 10948−10958.